Scanning Tunneling Microscopy – PHAS0051

L. Borek, A. Astrologia, K. Gharbi

Department of Physics and Astronomy, University College London (UCL), Gower St, London, WC1E 6BT

05/10/2021 – 03/01/2022

Word Count: 2727

Highly ordered pyrolytic Graphite (HOPG), Au (110) (Gold), MoS_2 (Molybdenum Disulfide), and TaS_2 (Tantalum Disulfide) were imaged using scanning tunnelling microscope operating in constant current mode. Atomic resolution was achieved for HOPG, MoS_2, and TaS_2 with typical 'a' lattice parameters being calculated for HOPG and MoS_2 as (2.8 ± 0.5) Å and (3.0 ± 0.5) Å respectively. A value for the S-layer to Mo-layer vertical separation was also obtained as (1.8 ± 0.6) Å, no atomic defects were observable in the imaged MoS_2. The imaged TaS_2 showed evidence of a charge density wave superlattice exhibiting a wavelength of (15.6 ± 0.6) nm.

I. Introduction

Scanning tunnelling microscopy has been a staple method of electrode micro-surface structure imaging since its development 40 years ago. STM has vast applications, for example in electrochemistry [1], it has proven useful in extracting electron transfer properties and electronic states of probed molecules, highlighting its potential in the field of pharmaceuticals via chemical probing. STM has also helped progress nanostructure fabrication which can be used to rectify defected surfaces and can aid in further research for nanostructures such as Graphene and Carbon Nanotubes [2].

STM functions via the utilisation of quantum tunnelling by which electrons tunnel between a conductive surface and an (ideally) atomically pointed wire after the application of a potential difference. If the probe tip is non-mono-atomically pointed, the wavefunctions of multiple tunnelling electrons will interfere and thus distort the 'true' signal that more accurately resembles the local density of states of the surface being imaged.

The probe tip in use consists of a Platinum Iridium alloy which possesses a flat density of states around the Fermi level and is chemically inert; [3] A. S. Darling emphasised Iridium-Platinum alloys for their malleability and extreme corrosion resistance, it does not oxidise in air at any temperature.

Concerning the workings of the STM in use, it operates in constant current mode (as opposed to constant height); the tunnelling current is kept constant by an electronic feedback loop to keep the tip-surface separation constant. The feedback loop minimises any difference between the set point (constant current value) and the tunnelling current by transmitting an actuating output signal via piezo elements which control the tip's motion. [4] These piezo elements are comprised of piezoelectric ceramics which change their outer dimensions when a bias is applied. The speed of the feedback loop's reaction to deviations is determined by I-gain, a higher I-gain equates to a higher reaction speed; the strength of proportionality between the feedback loop reaction and the deviations is determined by the P-gain. These parameters are known as the 'integral' and 'proportional' parts respectively.

When the bias voltage is applied, the Fermi level (thermodynamic work required to add one electron to a body) of the tunnelling destination decreases, creating an unoccupied state at the tip or sample (depending on field direction), allowing tunnelling electrons to occupy said state.

The tunnelling current is determined by a superposition of electron wave functions at the surface and tip; it's important to note that the tunnelling transmissivity decreases exponentially with tunnelling distance. [5] Trixler defines the transmission probability of an electron as [5]:

$$P = \frac{\left|\Psi_{(s)}\right|^2}{\left|\Psi_{(0)}\right|^2} = e^{-2ks} \qquad (1)$$

Where '0' and 's' are the end 'x' positions of the potential barrier and 'k' is the wave-function decay constant, written as [5]:

$$k = \frac{\sqrt{2m\Phi}}{\hbar} \quad (2)$$

Where $\Phi = V_0 - E_F$, demonstrated below:

Figure 1

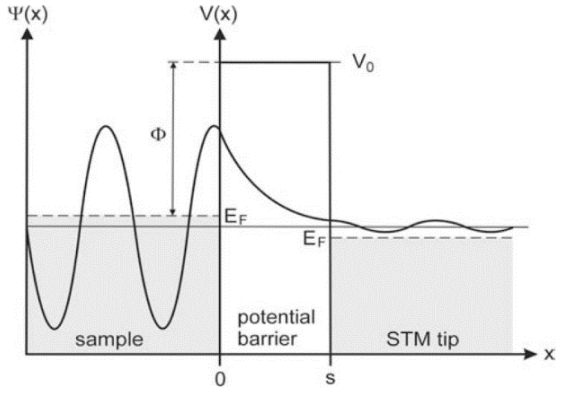

Figure 1. The tunnelling mechanism - a wave function is exponentially damped through a one-dimensional barrier where Φ is the tunnelling barrier height (local work function), V_0 is the vacuum level, E_F are the Fermi levels for the respective electrodes, s is the barrier width (from x=0 to x=s) [5].

Binnig and Rohrer write this otherwise as [6]:

$$J_T \propto V_T \, exp(-A\Phi^{1/2}s) \quad (3)$$

Where 'J_T' is the tunnelling current, 'V_T' is the vacuum level, 'A' ~ 1 if 'Φ' is measured in eV and 's' in Å.

If the potential barrier is small enough to yield a non-zero wave-function beyond it, tunnelling may occur because there exists a non-zero probability density for a particle to be located at that point.

[7] Hansma states that the current is proportional to the surface local density of states (LDOS) at the tip; the tip path maps out a contour of constant Fermi-level LDOS of the bare surface. Examining the properties of the LDOS can lead to the derivation of some general results concerning the STM image. For example, the resolution, normally defined in terms of an ideal image, an instrumental resolution function, and a resulting experimental image which is a convolution of the two.

From the materials being investigated, highly ordered pyrolytic graphite (HOPG) is unique because it is the only known fully conducting non-metal. It is comprised of a hexagonal lattice in which Carbon atoms are covalently bonded through weak nuclear forces (Van der Waals). [8] Colton emphasises the utility of HOPG as a benchmark for STM instrument test and calibration since HOPG can be readily cleaved to give large, atomically flat sample regions that are relatively clean and inert. Typical values for HOPG, are a bond length value of 1.42Å and lattice constant 'a' of 2.46Å [9] (Bond angle (C-C-C) of 120° would be expected due to the lattice's hexagonal nature). These represent the distance between 2 adjacent HOPG atoms and the distance between the hexagon / ring centres respectively.

Figure 2

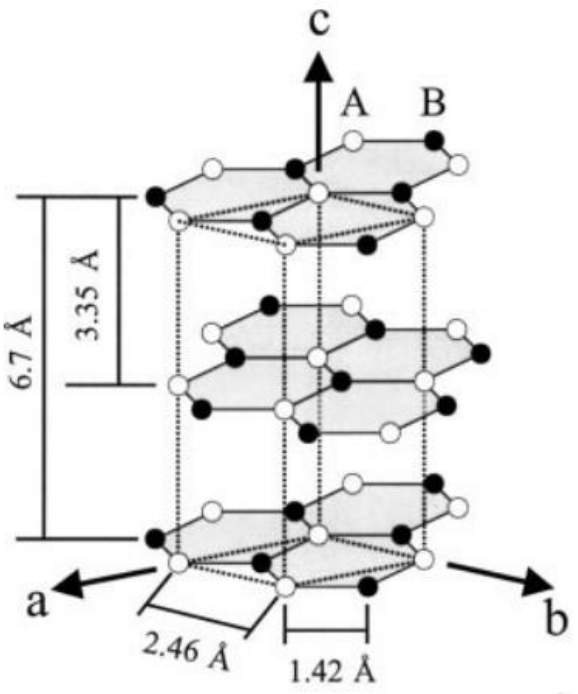

(i)

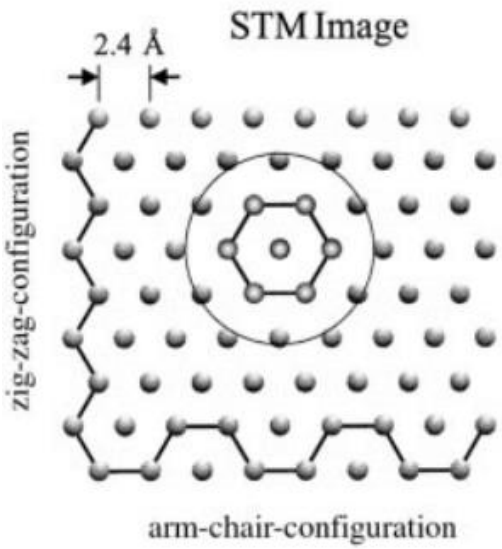

(ii)

Figure 2. (i). 3-D layered structure of HOPG showing lattice parameters
(ii). Basal layer perspective of HOPG [9]

Au (110) however (Gold), is comprised of Gold atoms bonded metallically in an FCC cubic structure, leading to a higher presence of free electrons; they are not shared as they are in covalent bonds. This makes Gold difficult to image at atomic resolution due to a uniform distribution of state densities across the surface which leads to a non-discernible lattice image.

Both MoS_2 and TaS_2 are transition-metal dichalcogenides (TMDs); they are hexagonally bonded compounds where each monolayer is comprised of 3 individual layers represented by a sandwich structure with a Sulphur layer at either monolayer boundary and a Molybdenum or Tantalum layer in between respectively. [10] 2-dimensional (monolayer) TMDS have gained attention due to their potential for energy storages because of their electrochemical properties.

Regarding MoS_2, images of MoS_2 crystals can often have defects as displayed below [11]:

Figure 3

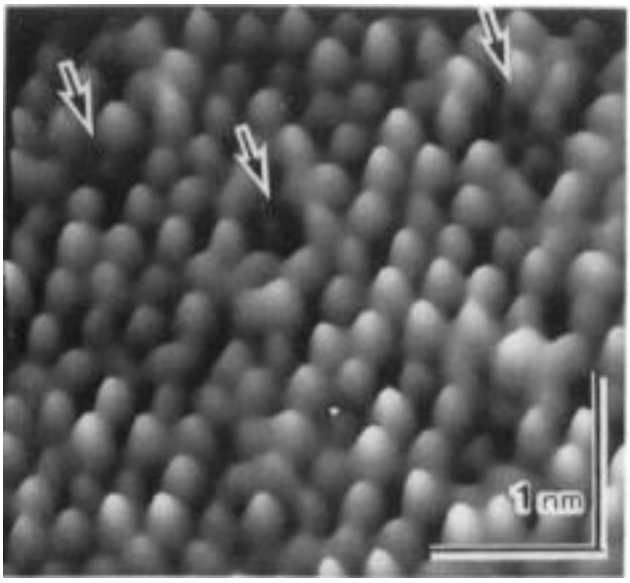

Figure 3. 3-Dimensinally imaged MoS_2 defects; generally taking the form of absent Sulphur atoms [11].

[12] An expected ‘a’ lattice parameter for MoS_2, commonly iterated, would be 3.16Å with a S-Mo vertical separation of 1.58Å.

TaS_2 comes in 3 polytypes, 1T, 2H, and 4hb (alternating T and H layers). Both 1T-TaS_2 and 4hb with T-type surface have the propensity to exhibit charge density waves at room temperature, iterated by Han et al. [13]. 4hb types with H-type surfaces are only capable of exhibiting charge density waves above a threshold of ~170mV [13] due to the relationship that dictates an increasing positive bias leads to an increasing tunnelling current via the electronic structure in the T-type subsurface layer, thus a CDW is observed in said subsurface layer and the CDW superlattice becomes indistinguishable from that observed on a T-type surface of 4hb-TaS_2. 2H-TaS_2 doesn’t exhibit CDWs throughout any later.

II. Method

The tip (Pt-Ir composite 80:20) was held in flat nose pliers and cut via wire cutters to a length of (1.0 ± 0.2) cm at approximately 45° and placed under the brass clamp in the STM station head. The tip’s sharpness can be

assessed via the Perspex cover. The sample was placed on a magnetic barrel and placed within 1cm of the tip; the Perspex cover was placed on the system to minimise the effect of air currents and thermal drift to an extent. Perspex is a better insulator and is more transparent than glass and so, this helps better identify a blunt tip and aids in minimising thermal and air current effects on the system. The barrel was advanced manually via the Perspex lens and the auto approach function was then used to bring the sample to within tunnelling current distance.

Figure 4

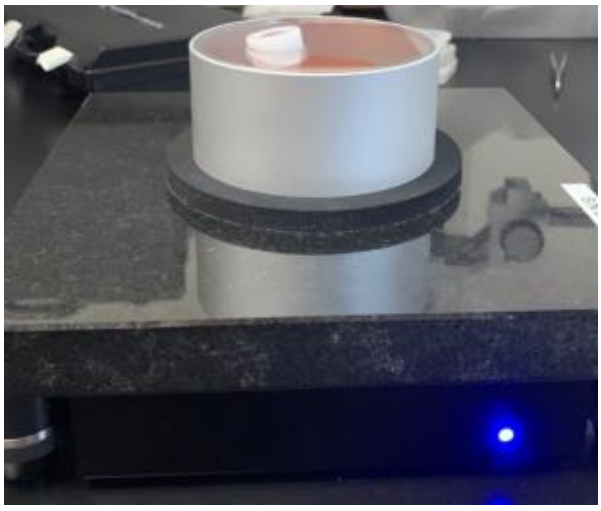

(i)

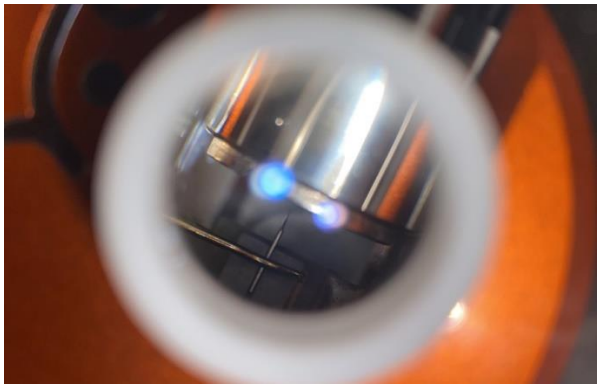

(ii)

Figure 4 (i). Nanosurf easyScan2 STM in use. (ii). Sample approaching tunnelling current distance of the tip clamped in the STM station head.

The I-gain, P-gain, and set point parameters should be specified according to the sample and a time per line chosen depending on the resolution being imaged (a higher time per results in less thermal drift but means that the tip isn't able to spend as long scanning the surface).

Adjusting the bias voltage is critical for ensuring a sufficient tunnelling current. Since Gold is highly electronegative and has a more homogenous distribution of electrons which are more tightly bound compared to HOPG, Gold consequently has a higher fermi energy than HOPG since more initial states are occupied; an increase in bias voltage from 50.1mV to 500mV is necessary to aid electron tunnelling by lowering this fermi level. However, if the bias is increased too much, there is an induced risk of photoelectrons being produced.

III. Provisional analysis

The raw images of atomically resolved lattice were imported to Gwyddion and 2D-filtering via Fast Fourier Transform (FFT) to 'clean' the images by highlighting primary periodicities in the image to keep; discarding other contributing 'noisy' signals. For images of lower resolution, there isn't so much a consistent presence of periodicities and thus FFT isn't necessary; only step alignment was used to balance the image contrast.

Lattice measurements were made in 2 different regions of the lattice to attempt to account for thermal drift. All obtained lattice images appeared slanted and stretched. Thermal drift is the most likely cause of this; it is the relative motion between the STM probe tip and the sample caused by thermal gradients and time-varying temperature, causing the STM framework to expand and contract. Since the distance between the tip and sample is 3 to 4 orders of magnitude larger than a typical scan size, small temperature changes can cause noticeable displacement between the tip and sample.

Figure 5

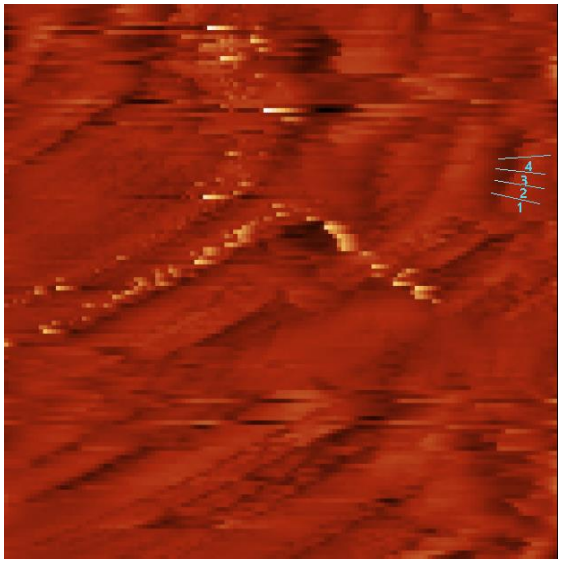

(i)

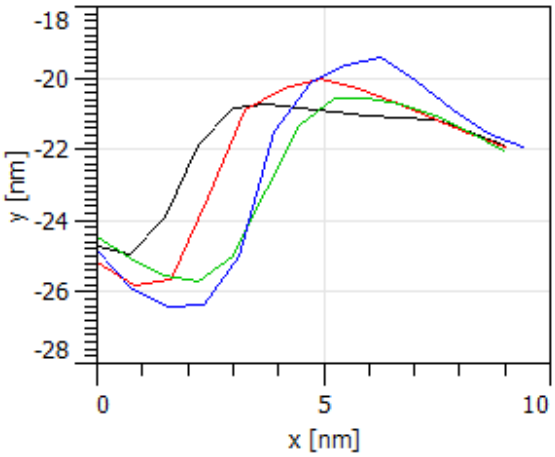

(ii)

Figure 5 (i). Gwyddion matching aligned unfiltered STM 100nm x 100nm resolution image of HOPG sample surface.
(ii). Arbitrary measurements across an appeared terrace step - lines 1-4 from (i) are represented as black, red, green, and blue respectively. Take 4 differences between the curve minimums and maximums, the measurements yielded an averaged terrace step height of (5.5 ± 0.2) nm.

Based on the findings of Lee et al [14]. in accordance with commonly accepted HOPG monoatomic step height values (displayed in Figure 2), the obtained value of (5.5 ± 0.2) nm from Figure 5 far exceeds the expected 0.34nm and thus can't be examined with dependability. It's likely that the noise present in the image takes precedent and distorts the distance. A resolution of 25-50nm x 25-50nm is much more likely to produce a better-quality image to obtain said value from.

Atomic resolution of HOPG was obtained, however not as discernibly as had been hoped for as seen in Figure 6.

Figure 6

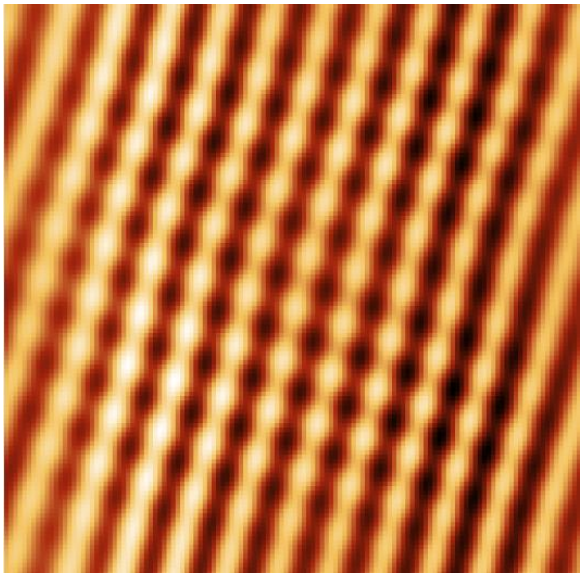

(i)

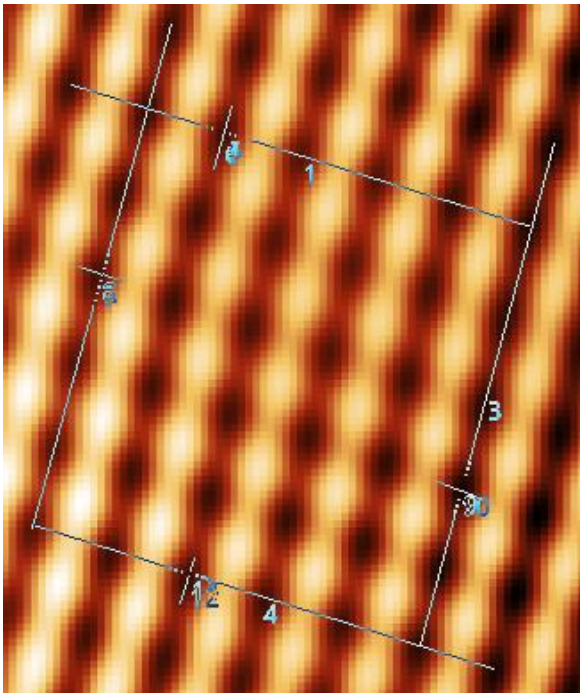

(ii)

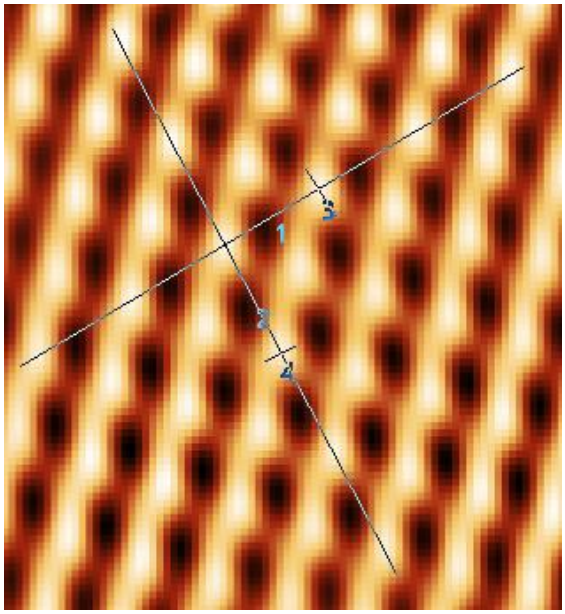

(iii)

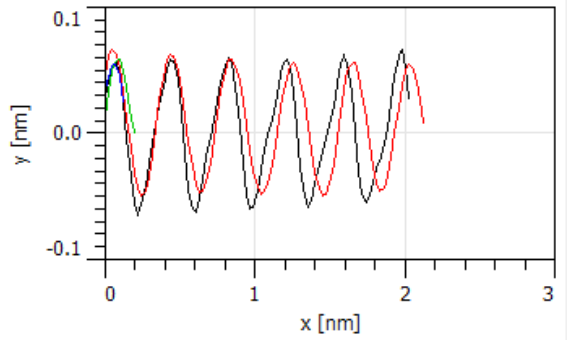

(iv)

Figure 6 (i). Gwyddion Fast-Fourier-Transform filtered STM 3.13nm x 3.13nm resolution image of HOPG sample surface.
(ii). Linear measurements across 2 planes of Sulphur atom adjacency in 2 regions of the HOPG lattice to account for some effect of thermal drift. The culmination of said measurements produced a value of (2.8 ± 0.5) Å for the distance between adjacent atomic ring centres, 'a'.
(iii). Linear measurements in 2 planes of Graphite LDOS maxima adjacency to determine a lattice parameter for the vertical distance between Graphite layers.
(iv). Graphical sequence of non-neighboured Carbon atoms by which vertical separations between surface and subsurface Carbon atoms were obtained, yielding an averaged value of (1.3 ± 0.6) Å. Lines 1-2 of (ii) in (iii) are represented by black and red respectively.

[3] Atamny et al. defined a confident value, iterated by multiple literatures, for the 'a' lattice parameter of HOPG as 2.46Å. The obtained value from the Figure 6 (ii) caption agrees with said value thus helps identify the experimental value to be dependable to an extent.

Figure 7

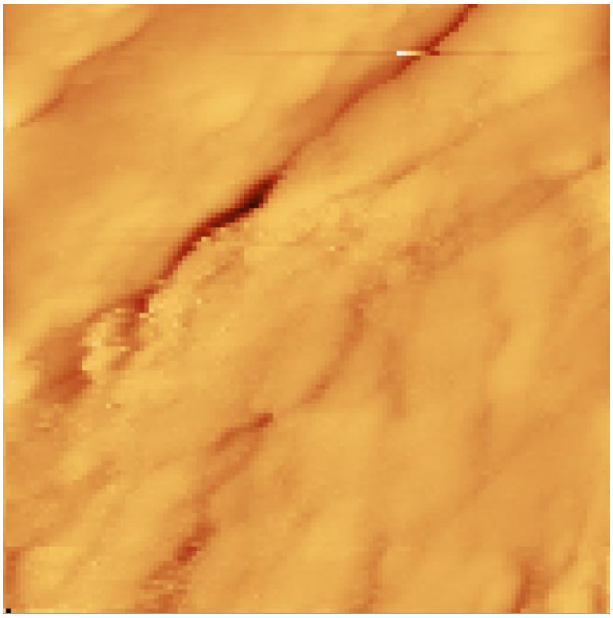

Figure 7. Gwyddion polynomial (4) aligned unfiltered STM 100nm x 100nm resolution image of Au (110) sample surface.

Au crystalline microstructures (grains) were observed and can be seen in Figure 7. Figure 8 displays some linear periodicity. A black crest can be seen which can either be interpreted as a surface crevice or a region of oxidisation / impurity; given that the rest of the image appears unoxidized, it's more likely to be a crevice. Figure 9 illustrates the topography of this.

Figure 8 (i). Arbitrarily drawn topography measurements on a 100nm x100nm resolution STM image of Gold (Figure).
(ii). Resultant z-axis profiles of the arbitrary lines in (i) where lines 1,3, and 5 are represented by black, red, and green respectively.

Figure 8

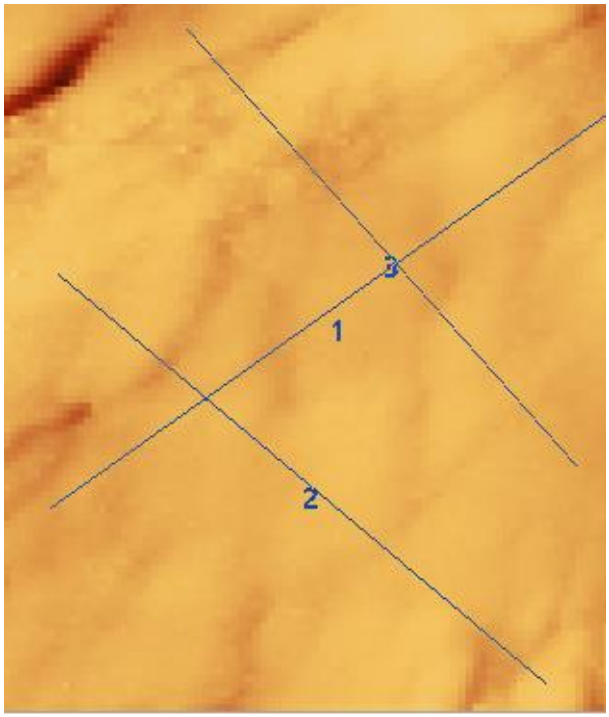

(i)

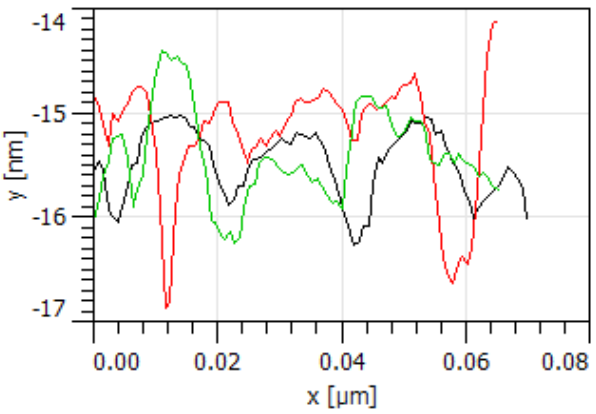

(ii)

Figure 9

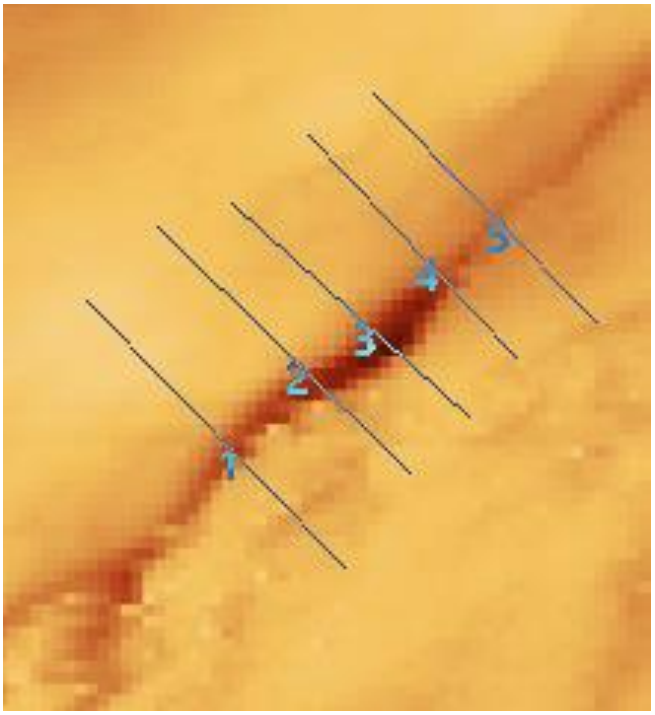

(i)

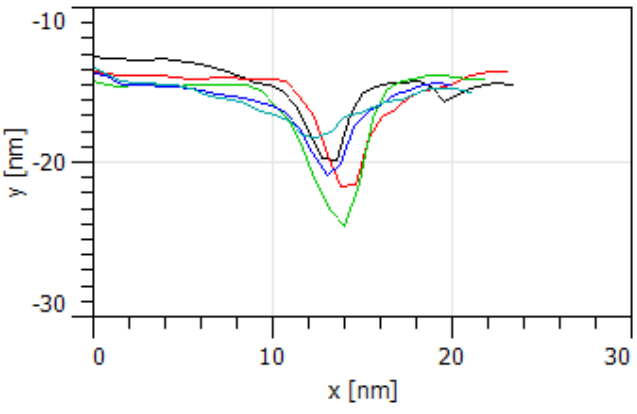

(ii)

Figure 9 (i). Topography measurements across what may be interpreted as a crevice or an oxidised region on a 100nm x 100nm resolution STM image of Gold (Figure 7). (ii). Resultant z-axis profiles of the arbitrary lines in (i) where lines 1-5 are represented by black, red, green, blue, and teal respectively.

Figure 10

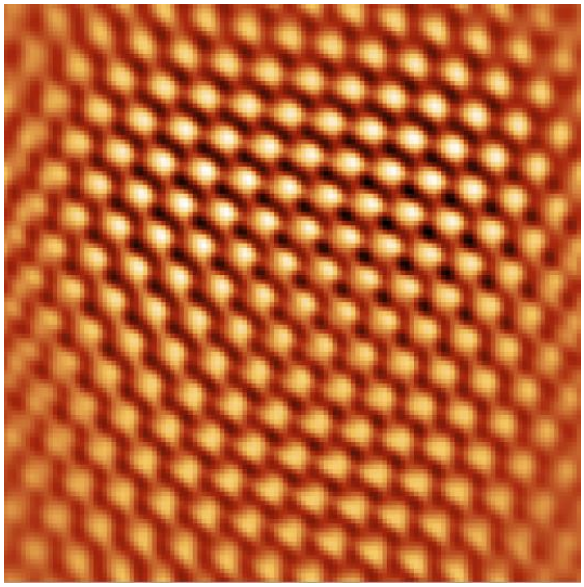

Figure 10. Gwyddion Fast-Fourier-Transform filtered STM 4nm x 4nm resolution image of MoS_2 sample surface.

MoS_2 defects were expected to take the form of Sulphur atoms absent from the surface S-layer represented by the bright lattice structure. No such defects are observable from the image. Figures 10 and 11 illustrate MoS_2 images and measurements.

Figure 11

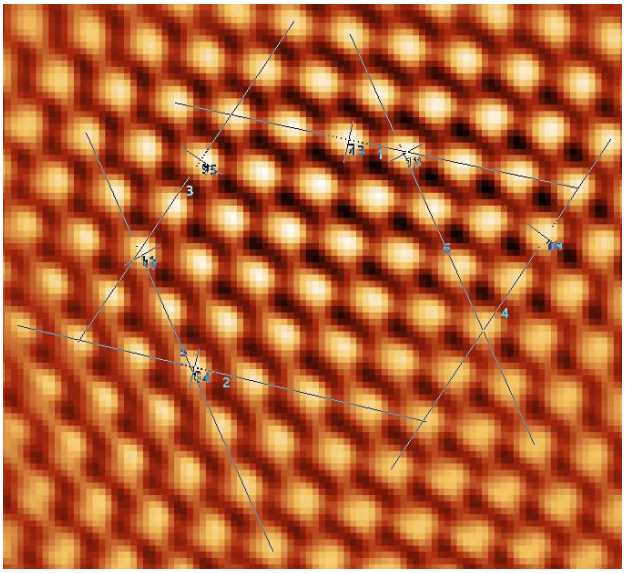

(i)

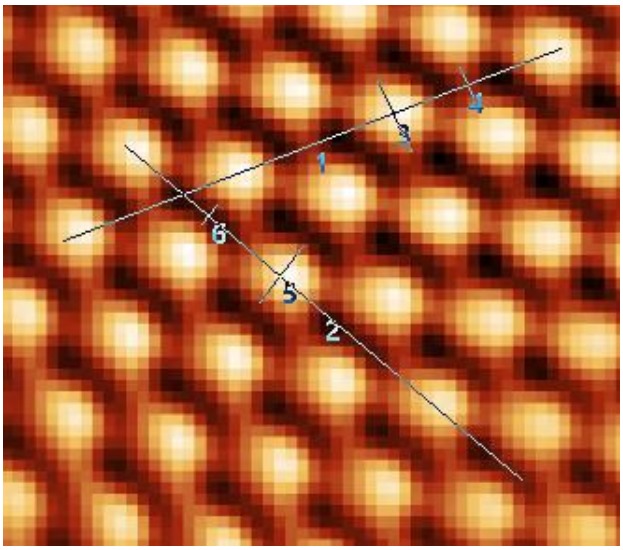

(ii)

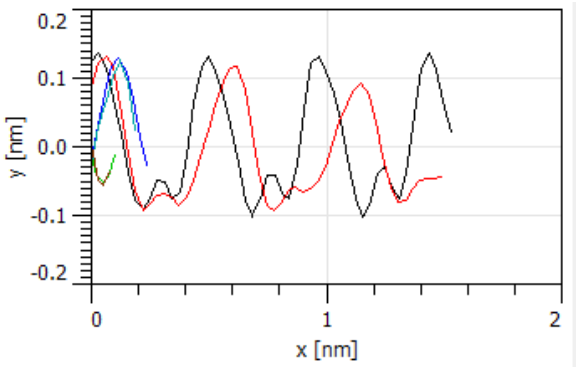

(iii)

Figure 11. (i). Measurements across 3 directions of Sulphur atom adjacency in 2 regions of the MoS_2. The culmination of said measurements produced a value of (3.0 ± 0.5) Å for the distance between adjacent Sulphur atom centres.
(ii). Arbitrary linear measurements in 2 planes of S-Mo atom x-axis adjacency to extract topography profiles and determine a lattice parameter for the vertical distance between Sulphur and Molybdenum atoms.
(iii). Graphical sequence of Sulphur and Molybdenum atoms - vertical differences between Sulphur and Molybdenum atom heights were averaged to obtain an S-layer to Mo-layer vertical separation of (1.8 ± 0.6) Å. Lines 1-2 of (ii) in (iii) are represented by black and red respectively.

Figure 12

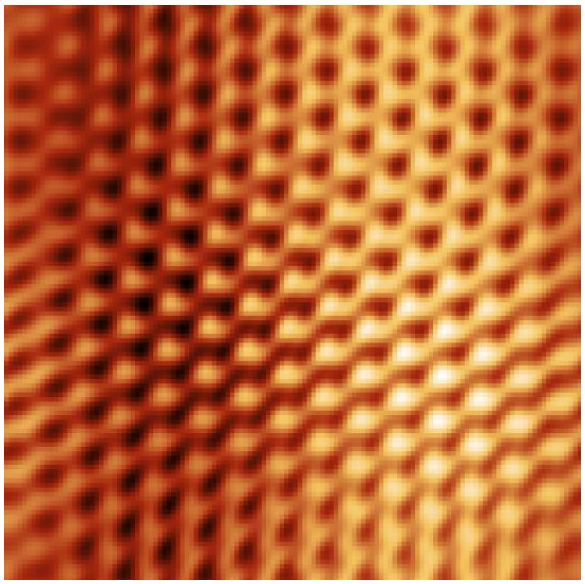

Figure 12. Gwyddion Fast-Fourier-Transform filtered STM 15x15nm^2 resolution image of TaS_2 sample surface.

For TaS_2, the image obtained (Figure 13) shows evidence of perturbation with the TaS_2 layer forming a CDW superlattice based off a stark contrast between image regions with seemingly increasing LDOS along the arrays of Sulphur surface atoms. The measured wavelength is defined in Figure 13 description.

Figure 13

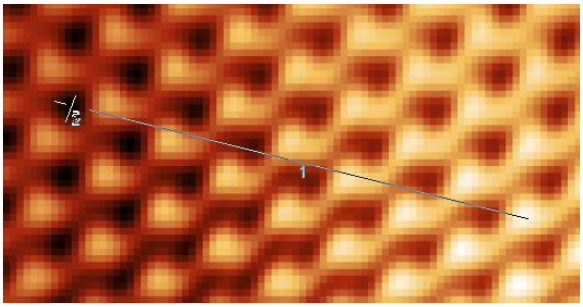

Figure 13. Radial measurement from the CDW superlattice local minimum to local maximum. The associated horizontal distance was interpreted as half a wavelength based on the standard form of a transverse wave; this yielded a wavelength value of (15.6 ± 0.6) nm.

Figure 14

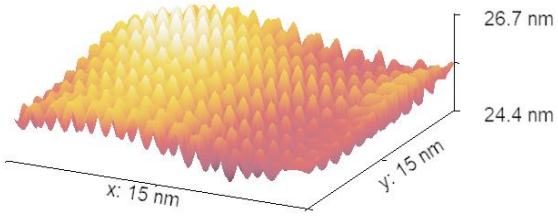

(i)

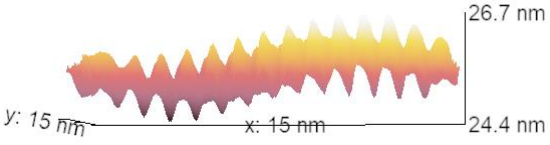

(ii)

Figure 14 (i) and (ii). Orientations of the 3-Dimensionally represented TaS_2 lattice utilised to identify the which individual atomic space

to consider as a CDW minimum and maximum.

These findings from Figures 13 and 14 confidently identify the imaged TaS_2 lattice to be of polytype 1T or 4hb with a 1T surface based on definitions given in the introduction.

IV. Conclusion

In summary, atomic resolution was obtained for both TMDs, MoS_2 and TaS_2, and HOPG. Two different approaches were taken to obtain a monolayer terrace step height for HOPG, both were considerably different to an expected height of 3.35Å (Figure 2).

The only values obtained that agree to an extent with literature values were those obtained for MoS_2 and the 'a' lattice parameter of HOPG.

Atomic resolution was not obtained for the Gold sample, most likely attributed to the fact that a very uniform distribution of state densities causes the tip to produce a scan which doesn't produce distinguishable lattice features.

No atomic defects were observed within the MoS_2 lattice; this meant that minimal information could be discerned about the sample's electronic properties since it is the implications put forward by the presence of such defects that allow for the extraction of such information. A CDW TaS_2 superlattice was observed with literature-based grounding for a dependable wavelength.

To improve this experiment, performing it in a vacuum at very low temperatures would aid in reducing thermal drift. Electrolytically etching the tip in addition to annealing surfaces would also aid in measurement precision.

References

1. N. J. Tao, C. Z. Li, H. X. He. (2000, Oct). "Scanning tunneling microscopy applications in electrochemistry - beyond imaging". *Journal of Electroanalytical Chemistry* [Online]. vol. 492, issue 2, pp.81-93. Available: https://www.sciencedirect.com/science/article/pii/S0022072800002953 [Accessed: Dec 26, 2021].
2. X. Cheng. (2014) "Nanostructures: fabrication and applications". *Nanolithography* [Online]. pp.348-375. Available: https://www.sciencedirect.com/science/article/pii/B9780857095008500105[Accessed: Dec 26, 2021].
3. A.S. Darling. (1960). "Iridium Platinum Alloys: A critical review of their Constitution and Properties". , *Platinum Metals Review* [Online]. vol. 4, issue 1, pp.483–488. Available: https://www.technology.matthey.com/article/4/1/18-26/ [Accessed: Dec 28, 2021].
4. J. F. Wolf. (2000, Jan. 4). *Scanning Tunneling Microscopy of 2D-Molecule Crystals at the Solid/Liquid Interface* [Online]. Available: https://www.analytik.ethz.ch/praktika/analytisch/stm/humboldt.pdf [Accessed: Dec 28, 2021].
5. F. Trixler. (2013, Aug). "Quantum Tunnelling to the Origin and the Evolution of Life". *Current Organic Chemistry* [Online]. vol. 17, issue 16, pp. 1758-1770. Available: https://www.ncbi.nlm.nih.gov/pmc/articles/PMC3768233/[Accessed: Dec 30, 2021].
6. G. Binnig, H. Rohrer, "Scanning tunneling microscopy", Surface Science, Volume 126, Issues 1-3, 1983, pp.236-244, ISSN 0039-6028. Available:https://www.sciencedirect.com/science/article/pii/0039602885901207 [Accessed: Dec 30, 2022].
7. P. K. Hansma, J. Tersoff. (1987, Sep). "Scanning tunnelling microscopy". *Journal of applied physics* [Online]. vol.61, issue 2, pp. 01–24. Available: https://aip-scitation-org.libproxy.ucl.ac.uk/doi/10.1063/1.338189 [Accessed: Dec 30, 2021].
8. R.J. Colton, S.M. Baker, R.J. Driscoll, M.G. Youngquist and J.D. Baldeschwieler. "Imaging graphite in air by scanning tunneling microscopy: Role of the tip". Journey of Vacuum Science & TechnologyA 6, 349 (1988) [Online]. Volume 6, Issue 2. Available:

https://avs.scitation.org/doi/abs/10.1116/1.575411 [Accessed: Jan 03, 2022].
9. F. Atamny, O. Spillecke, R. Schlögl. "On the STM imaging contrast of graphite: towards a 'true' atomic resolution". Physical chemistry chemical physics: PCCP [Online]. Vol. 1, issue 17, pp.4414-4415. Available: https://pubs.rsc.org/en/content/articlelanding/1999/CP/a904657g [Accessed: Jan 03, 2022].
10. Wonbong Choi, Nitin Choudhary, Gang Hee Han, Juhong Park, Deji Akinwande, Young Hee Lee, "Recent development of two-dimensional transition metal dichalcogenides and their applications", Materials Today [Online], Volume 20, Issue 3, 2017, pp. 116-130, ISSN 1369-7021. Available:https://www.sciencedirect.com/science/article/pii/S1369702116302917 [Accessed: Jan 03, 2022].
11. S. Hosoki, S. Hosaka, T. Hasegawa, (1992). "Surface modification of MoS_2 using an STM". Applied Surface Science [Online]. vol. 60, pp.643-647, 1992. [Online]. Available: https://www.semanticscholar.org/paper/Surface-modification-of-MoS2-using-an-STM-Hosoki-Hosaka/2df0b167325dd66985a6e71c458a75a81ae033ef [Accessed: 03 Jan 2022].
12. M. Li, et al., (2016, Apr). "Experimental study and modelling of atomic-scale friction in zigzag and armchair lattice orientations of MoS_2. *Science and technology of advanced materials* [Online]. vol. 17, issue 1, pp.189-199. Available: https://www.ncbi.nlm.nih.gov/pmc/articles/PMC5101872/ [Accessed: 03 Jan 2022].
13. W. Han et al., (1994, Nov). "Bias-dependent STM images of charge-density waves on TaS_2". *Physical review. B, Condensed matter* [Online]. vol. 50, issue 19, pp.14746-14749. Available: https://journals.aps.org/prb/abstract/10.1103/PhysRevB.50.14746 [Accessed: 03 Jan 2022].
14. H. Lee, H.B.R. Lee, S. Kwon, M. Salmeron, J.Y. Park. (2015, Mar). "Internal and External Atomic Steps in Graphite Exhibit Dramatically Different Physical and Chemical Properties". *ACS Nano* [Online]. vol. 9, issue 4, pp.3814-3819. Available: https://pubs.acs.org/doi/10.1021/nn506755p [Accessed: Jan 03, 2022].